Int. J. Electrochem. Sci., 13 **(2018)** 2136 – 2153, doi: 10.20964/2018.02.76

International Journal of ELECTROCHEMICAL SCIENCE
www.electrochemsci.org

Histidine and histidine dimer as green inhibitors for carbon steel in 3wt% sodium chloride solution; Electrochemical, XPS and Quantum chemical calculation studies

Liyun Zhang[1,2], *Shihong Zhang*[2], *Yi He*[1,2,3,*], *Ranran Yang*[2], *Lan Ma*[2], *Yunqing Xia*[2], *Ze He*[2,*]

[1] State Key Lab of Oil and Gas Reservoir Geology and Exploitation, Southwest Petroleum University, 8 Xindu Avenue, Chengdu, Sichuan 610500, P R of China
[2] School of Chemistry and Chemical Engineering, Southwest Petroleum University, 8 Xindu Avenue, Chengdu, Sichuan 610500, P R of China
[3] Oil & Gas Field Applied Chemistry Key Laboratory of Sichuan Province, Chengdu, 610500, China
[*]E-mail: heyi@swpu.edu.cn, heze1313@hotmail.com

Received: 28 October 2017 / *Accepted:* 14 December 2017 / *Published:* 28 December 2017

Histidine (ethyl-2-amino-3-(1H-imidazol-2-yl) propanoate), a raw material, was used to synthesize a new green histidine dimer (2-(2-amino-3-(1H-imidazol-2-yl)propanamido)-3-(1H-imidazol-2-yl)propanoic acid) inhibitor. The corrosion inhibition properties of histidine and the histidine dimer for N80 steel were explored in 3 wt% NaCl solution through weight loss experiments and electrochemistry experiments (including potentiodynamic polarization tests and electrochemical impedance spectroscopy (EIS)). The surface morphology and elemental composition of corroded N80 steels were analysed by scanning electronic microscopy (SEM), energy dispersive spectroscopy (EDS) and X-ray photoelectron spectroscopy (XPS). Weight loss experiments showed that the histidine dimer has better inhibitory performance than histidine. When the dosages of histidine and the histidine dimer reached 250 mg/L, the inhibition efficiency reached maximum values of 86% and 94%, respectively. In addition, the results of Scanning Electron Microscopy (SEM) and X-ray photoelectron spectroscopy (XPS) further confirmed that histidine and the histidine dimer can form a protective layer on the surface of N80 steel. The inhibition mechanism and molecular structure of histidine and the histidine dimer were analysed by quantum chemical calculation methods, and the results showed that the better inhibition efficiency of the histidine dimer may be due to the increase of adsorption sites on the histidine dimer compared with histidine, which facilitates adsorption on the surface of N80 steel. Moreover, the examination of adsorption properties showed that the adsorption behaviour of histidine and the histidine dimer on N80 steel followed the Langmuir adsorption isotherm model.

Keywords: Histidine dimer, green corrosion inhibitor, carbon steel, chloride sodium.

1. INTRODUCTION

The corrosion of carbon steel generally occurs in the process of industrial production and frequently poses many serious problems that affect the safety of the operator and cause a great amount of economic loss[1]. Local corrosion is a common phenomenon of metal corrosion. Salt solution leads to the localized corrosion of carbon steel[2, 3]. Moreover, some previous studies have shown that the chloride ions of chloride solutions lead to pitting corrosion on the metal surface when placing carbon steel in a chlorine solution [4-6]. Cáceres [7] demonstrated that most holes on steels appear around the destroyed areas and further contribute to the local dissolution of carbon steel in the NaCl solution. In these conditions (including seawater and some industrial environments), the oxygen reduction reaction (ORR) on the steel's surface may cause large-scale corrosion damage to unprotected carbon steels[8, 9]. One of the main methods used to protect carbon steel is the use of corrosion inhibitors in neutral NaCl solutions [10], which can retard metal corrosion at the interface of the corrosion media and the steel's surface. In previous studies, organic compounds containing nitrogen, oxygen or sulphur atoms have been widely used as potential inhibitors [11-17]. However, most of them are synthetic chemicals with biologic toxicity and are too hazardous for human beings and the environment. For this reason, developing a non-toxic, environmentally friendly and cheaper corrosion inhibitor is warranted.

A series of amino acids as green inhibitors were recently reported to be non-toxic and biodegradable[18] and showed good corrosion inhibition with carbon steel[19-23], iron[24], copper[25, 26], aluminium[27], vanadium and alloys[28]. Compared to other amino acids, histidine contains not only carboxyl and amino groups but also an imidazole ring. Additional groups and an imidazole ring increase the electron density of inhibitors and have shown a greater inhibition effect because they offer a pair of lone electrons or have low-energy empty orbitals to receive electrons, forming a physical barrier on the metal surface via adsorption reaction [29-31]. Fu [32] first explored L-histidine as a corrosion inhibitor and its inhibitory performance for mild steel in HCl solutions. Bobina [33] also studied L-histidine as a corrosion inhibitor for mild steel in a weak acid media containing acetic acid/sodium acetate. The results showed that the maximum value of the inhibitory efficiency of L-histidine could reach 81.6% in the corrosion media. In addition, most current green inhibitors were investigated in acid solution, such as hydrochloride acid[18, 19, 32, 34], sulfuric acid[35], and nitric acid[36]. However, few studies have focused on the application of green inhibitors in sodium chloride solution. Furthermore, the synthesis of a histidine dimer as a green inhibitor for N80 steel in 3wt% sodium chloride solution has not yet been reported.

In this paper, we synthesized a histidine dimer (2-(2-amino-3-(1H-imidazol-2-yl)propanamido)-3-(1H-imidazol-2-yl)propanoic acid) to increase the number of molecular adsorption sites to obtain a more effective and green inhibitor. Moreover, the inhibitory performance of histidine and histidine dimer for N80 steel in 3 wt% NaCl solution was evaluated through weight loss and electrochemical tests. The surface morphology and elemental composition of corroded N80 steel were analysed utilizing scanning electronic microscopy (SEM), energy disperse spectrometry (EDS) and X-ray photoelectron spectroscopy (XPS). Furthermore, the inhibitory mechanisms of histidine and a histidine dimer for N80 steel in 3 wt% NaCl solutions were clarified using quantum chemical calculations.

2. EXPERIMENTAL

2.1. Materials

In this study, Carbon steel (N80) of chemical composition (0.24% C, 0.22 %Si, 1.19%Mn, 0.013% P, 0.004 %S, 0.015% V, 0.0036 %Cr, the remainder Fe) (22 mm×12mm×2mm) with a hole diameter of 3mm. Prior to experiment, the surface of steel is polished by mechanically grounding with 400, 800, 1000 and 1200 emery paper, washed orderly with distilled water, ethanol and acetone. During the investigation, 3 wt % sodium chloride solution was the corrosive medium. Histidine (ethyl-2-amino-3-(1H-imidazol-2-yl) propanoate), ethanol, acetone and sodium chloride (NaCl) were supplied by Chemical Reagent Factory (Chengdu, China). All chemical reagents were of analytical grade and were used without further purification. Deionized water with a resistance of 18.2 MX cm was provided by a UPC-III water purification system.

2.2. Synthesis of histidine dimer (2-(2-amino-3-(1H-imidazol-2-yl) propanamido)-3-(1H-imidazol-2-yl) propanoic acid)

The molecular structure of the histidine dimer is shown in Fig 1. At first, 2 g histidine was added to a 250 mL three neck flask and 40 mL absolute ethanol was poured into the flask and stirred at 323.15 K. Then, concentrated hydrochloric acid was added into the mixture drop by drop until the histidine dimer was completely soluble. The mixture continued to react for 30 min. Histidine ethyl ester hydrochloride (HEEH) was obtained by removing excess ethanol. Next, the histidine ethyl ester hydrochloride was dissolved in the distilled water, 30wt% NaCl solution was added and the pH value was adjusted to 8-9. Then, a white precipitate of histidine ethyl ester was obtained. Subsequently, 10 mL distilled water was mixed with the histidine ethyl ester and an equal molar concentration of histidine dimer. Then, triethylamine (acid-binding agent) and DMAP were added to the mixture. The mixture was stirred at 323.15 K for 24 hours. After the reaction, the solvent was distilled under a vacuum. A small amount of water was used to dissolve the precipitate, and the pH value was adjusted to 2-3 with hydrochloric acid. Finally, the solution was extracted by ethyl acetate, and the supernatant was dried by anhydrous magnesium sulphate overnight. The solvent was distilled under a vacuum, and the product was obtained by column chromatography. The eluent of petroleum ether: ethyl acetate is 2:1. The synthesis of the histidine dimer is shown in Scheme 2.

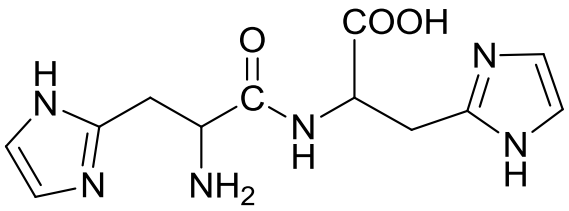

Scheme 1. Structural formula of Histidine dimer

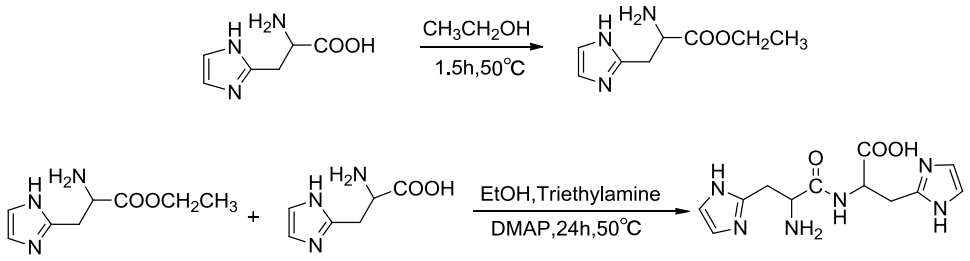

Scheme 2. Synthesis route of Histidine dimer

2.3 Structure characterization

We confirmed the chemical structure of composition through Fourier Transform Infrared Spectrometer (FT-IR) (WQF520) and Nuclear Magnetic Resonance Spectroscopy(NMR) (Bruker AVANCE Ⅲ HD 400). The ^{1}H NMR test for histidine dimer was conducted under $CDCl_3$ atmosphere.

2.4. Weight loss

The prepared specimens of N80 carbon steel were accurately weighed and the surface area was computed. These specimens were immersed in the 3wt% NaCl solution containing the different concentrations of inhibitors, and the temperature of the solution was maintained at 298 K. After a specific time period, the specimens were removed, washed, dried, and weighed accurately. The average weight loss of the three parallel specimens was obtained. The inhibition efficiency (η) and the degree of surface coverage (θ) at different concentrations of investigated inhibitors on the corrosion of specimens were calculated as shown in Eqs. (1), (2) and (3)[37].

$$r_{corr} = \frac{\Delta m}{ST} \quad (1)$$

$$\eta(\%) = \frac{r^0_{corr} - r_{corr}}{r^0_{corr}} \times 100 \quad (2)$$

$$\theta = \frac{r^0_{corr} - r_{corr}}{r^0_{corr}} \quad (3)$$

Where Δm is the average weight loss of the three parallel specimens, *S* and *T* are the area of metal surface and immersing time in corrosive medium, respectively. r^0_{corr} and r_{corr} represent the corrosion rate of N80 steel in 3wt% NaCl without and with inhibitor solution, separately.

2.5. Electrochemical experiments

An electrochemical work station including a computer-controlled system (CorrTest Company, Wuhan, China) and a conventional three-electrode compartment were employed in the experiment. The N80 carbon steel was used as a working electrode (WE) along with a platinum counter electrode as the auxiliary electrode (AE) and a saturated calomel electrode (SCE) as the reference electrode

(RE). The corrosive medium was the 3 wt% sodium chloride (NaCl) solution containing the different concentrations of inhibitor. It was maintained at 298 K.

Polarization measurements-the polarization measurements were carried out at the potential range from -0.80 to -0.25 V vs. SCE with a scanning rate of 1 $mV{\cdot}s^{-1}$. The linear Tafel segments of the anodic and cathodic curves were extrapolated to the corrosion potential (E_{corr}) to obtain the corrosion current density (i_{corr}). The inhibition efficiency $\eta_p(\%)$ and surface coverage (θ) was determined by Eqs. (4) and (5).

$$\eta_p(\%) = \frac{i^0_{corr} - i_{corr}}{i^0_{corr}} \text{ x } 100 \quad (4)$$

$$\theta = \frac{i^0_{corr} - i_{corr}}{i^0_{corr}} \quad (5)$$

Where i^0_{corr} and i_{corr} represent the corrosion current density in absence and presence of inhibitor, respectively[38, 39].

Electrochemical impedance spectroscopy measurements-EIS were tested in the frequency from 100 kHz to 0.01 Hz at alternating current amplitude of 5 mV sine wave. The software ZSimpWin was used to analyze the impedance data, inhibition efficiency $\eta_z(\%)$ calculated by the following Eq. (6):

$$\eta_z\ (\%) = \frac{R_{ct} - R^0_{ct}}{R_{ct}} \times 100 \quad (6)$$

where R^0_{ct} and R_{ct} are charge transfer resistances in the corrosive medium without and with the different concentration of inhibitor, respectively[38].

2.6. Surface analysis

To investigate the morphology and elemental composition of corrode steels, the specimens were treated in 3wt% sodium chloride solution without or with 0.15g /L inhibitors at 298 K for 72 hours, followed by washing with distilled water under ultrasound for several minutes, and placed into dryer. Then they were characterized by the scanning electron microscope (JSM-7500F) and X-ray photoelectron spectroscopy (XPS) (KRATOS, XSAM800).

2.7. Quantum chemistry calculations

Geometric optimization, orbital energy calculations, chemical potentials, Hirshfeld charges, and the corresponding Condensed Fukui functions of inhibitor molecules were performed using all based on the B3LYP-D3 (BJ) functional combination of 6-311G * basis sets (for C, O, N) and 6-31G * basis sets (For H) using Gaussian 03 program package, and then the trajectory graphics were drawn by Multiwfn + VMD.

3. RESULT AND DISCUSSION

3.1 FTIR

The FT-IR of histidine and histidine dimer were showed in Fig 1 (a) and Fig 1 (b), respectively. The peak around 3419 cm $^{-1}$was stretching vibration of N-H and the peaks of 1612 cm^{-1} was the C = O stretching vibration peak in Fig 1 (b) ,which confirmed the presence of an amide bond[17]. The peak observed near 1335cm^{-1} was the stretching vibration of C-N of imidazoline ring structure, other peaks at 1300~1200 cm^{-1} were due to the characteristic absorption peaks of C-N group of imidazole ring in Fig 1 (b). These results proved histidine dimer was successfully synthesized.

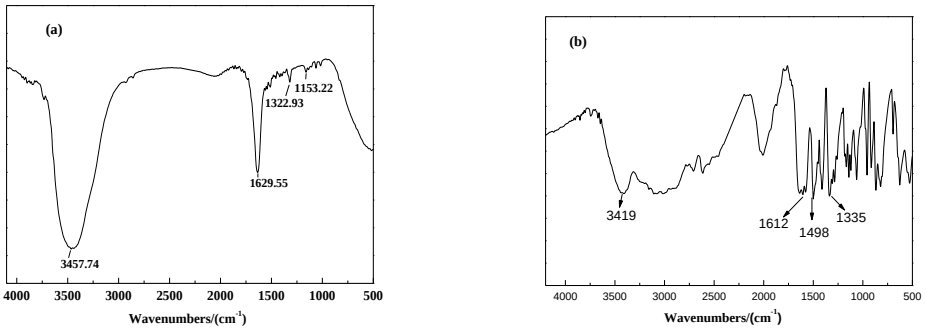

Figure 1. FTIR spectrum of Histidine(a) and Histidine dimer(b)

3.2 The spectrum of ^{1}H NMR

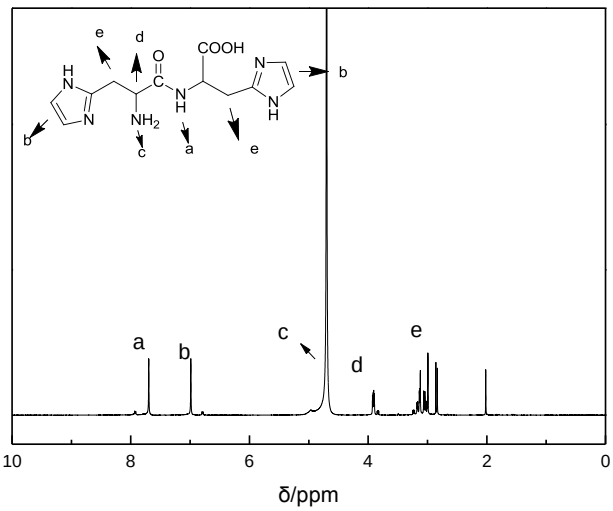

Figure 2. ^{1}H NMR spectra of Histidine dimer in $CDCl_3$

The result of ^{1}H NMR of histidine dimer showed Fig 2, δ=7.81 ppm are corresponding to the chemical shift of amide groups,δ=6.86 ppm represented the chemical shift of the protons on the two imidazoline rings [22]. δ=4.89 ppm signified the chemical shift of the amino groups, around δ=3.17

indicated the chemical shift of the Methylene beside the two imidazoline rings. The signals located at broad chemical shifts in the region of 3.91-3.8 ppm were attributable to chemical shift of the inner methylidyne. Therefore, it can be conclude that histidine dimer has been successfully synthesized.

3.3 Weight loss studies

Table 1 showed result of weight loss test of N80 carbon steel was immersed in 3wt% sodium chloride solution contained the different concentration (0.05, 0.1, 0.15, 0.2, 0.25 g/L) of inhibitors at 298K for72 hours. θ is the coverage of the corrosion inhibitor on the surface of the steel sheet, and η is the corrosion inhibition efficiency. When the dosage of histidine and histidine dimer both have reached 0.25 g/L, the value of inhibition efficiency (η) reached 86% and 94%, respectively.

Table 1. The parameters of weight loss experiment for N80 carbon steel in the 3wt% NaCl solution with various concentrations of histidine and histidine dimer at 298 K.

C(mg·L^{-1})	histidine		histidine dimer	
	η **(%)**	θ (%)	η **(%)**	θ (%)
50	76	76	81	81
100	80	80	88	88
150	82	82	90	90
200	86	86	93	93
250	86	86	94	94

At the same time, the results showed that the histidine and histidine dimer both can mitigate the corrosion of N80 steel in 3 wt% NaCl solution well, but histidine dimer has more inhibition efficiency at the same dosage. It could be that histidine dimer has bigger molecular size and more high electron density of active groups and atoms [40], histidine dimer molecules with more oxygen, amino groups, imidazoline ring functional can more easily adsorb on steel surface to form a compact protective layer to reduce the corrosion of N80 steel in 3 wt% NaCl [29]. At the same time, we can see that inhibition efficiencies of histidine and its dimer corrosion inhibitor did not change much at several concentrations above 0.1 g / L, it may be due to corrosion inhibitor molecules have basically covered the metal surface, so with the increase in concentration of corrosion inhibitor, the change of corrosion inhibitor efficient is not obvious.

3.4 Electrochemical analysis

3.4.1 Potentiodynamic polarization tests

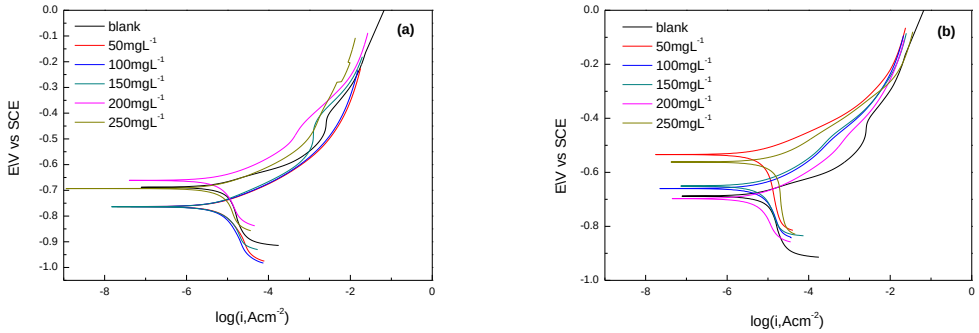

Figure 3. Polarization curves for the N80 carbon steel in 3 wt% NaCl solution in the presence of different dosages of histidine and histidine dimer at 298 K (a—histidine, b--histidine dimer)

Fig 3(a, b) displays polarization curves for N80 in 3wt% NaCl with different concentrations of histidine and histidine dimer at 298K. It can be seen from Fig 3 (a, b) that the corrosion potential both moves toward the negative direction after adding histidine and its dimer, and then the corrosion current density also decreases, it indicated that inhibitor formed a adsorption layer on steel surface, which obstructed the contact between the corrosion medium and steel sheet and has a good corrosion inhibition efficient. But histidine dimer has lower corrosion current density, it indicated that histidine dimer has a better inhibition property.

Table 2. The electrochemical kinetic parameters for polarization curves

Inhibitors	C(mg·L^{-1})	E_{corr}(mV vs SCE)	β_c(mV·dec^{-1})	β_a(mV·dec^{-1})	i_{corr}(mA·cm^{-2})	η_p(%)
Histidine	0	-686	-48.2	95.0	1.7×10^{-4}	--
	50	-720	-189.6	74.7	1.5×10^{-5}	90.8
	100	-760	-239.7	71.3	1.5×10^{-5}	91.1
	150	-754	-188.5	67.4	1.3×10^{-5}	92.2
	200	-663	-200.1	66.2	1.3×10^{-5}	92.4
	250	-695	-155.9	65.0	1.2×10^{-5}	93.1
Histidine dimer	50	-525	-482.7	63.6	1.7×10^{-5}	89.6
	100	-671	-249.1	95.7	1.7×10^{-5}	90.1
	150	-662	-229.7	92.8	1.5×10^{-5}	91.0
	200	-700	-132.0	65.8	0.9×10^{-5}	94.9
	250	-568	-397.1	95.3	0.8×10^{-5}	95.2

The polarization parameters such as corrosion potential (E_{corr}), corrosion current density(i_{corr}) and anodic (β_a)/cathodic (β_c) Tafel slopes were presented in Table 2. It can be observed that the values

of i_{corr} was decreased with the increasing of the concentration of histidine and histidine dimer. There is no explicit trend in the range of E_{corr} values with concentration change of histidine and histidine dimer. However, after adding inhibitor, cathode Tafel slopes (β_c) and anode Tafel slopes (β_a) both shifted with the concentration of histidine and histidine dimer relative to corrosion potential of blank sample. For these two inhibitors, the changes of cathodic slope are more pronounced than anodic slope. It indicated that both histidine and histidine dimer are attributed to mixed-type with predominantly cathodic action. [41].

The changes of anodic slope(β_a) with addition of histidine and dimer suggest that the two inhibitors adsorb on N80 steel surface and cover the reaction sites of metal surface. Meanwhile, cathodic slope (β_c) values change with the addition of histidine and histidine dimer suggesting that mechanism of hydrogen evolution reaction is changed in the presence of two inhibitors. This result illustrated that histidine and histidine dimer both can form a barrier on metal surface and protect steel from corrosion in salt solution. Based on the analysis of polarization tests, the results obtained from polarization method is coincident with the weight loss result [38, 42].

3.4.2 Electrochemical impedance spectroscopy (EIS)

Electrochemical impedance spectroscopy was used to examine the corrosion inhibition processes of N80 carbon steel in inhibited and uninhibited solution.

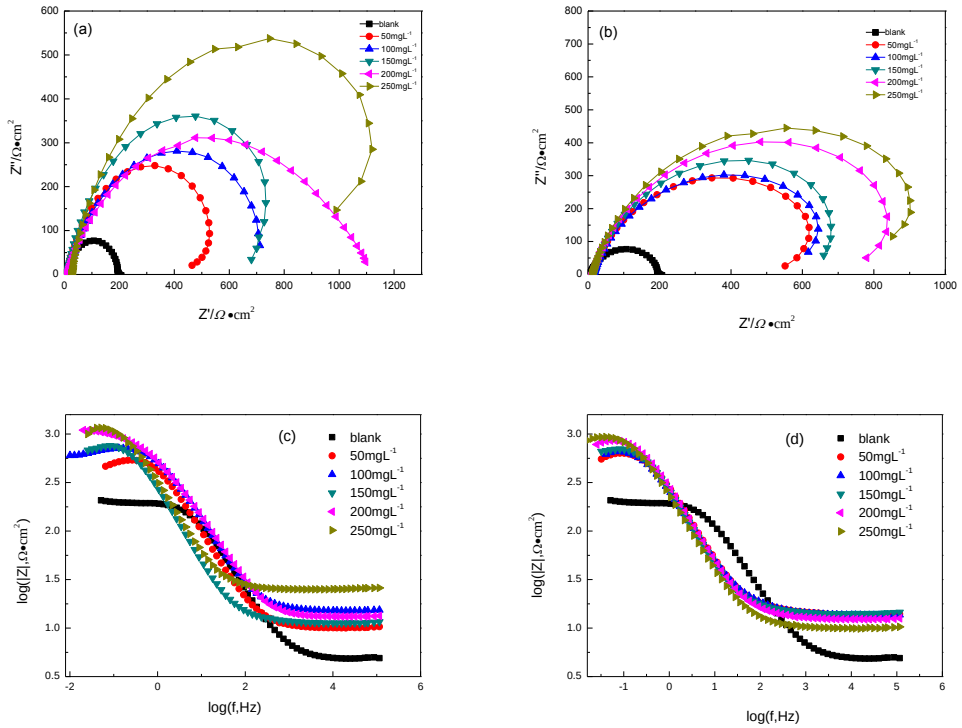

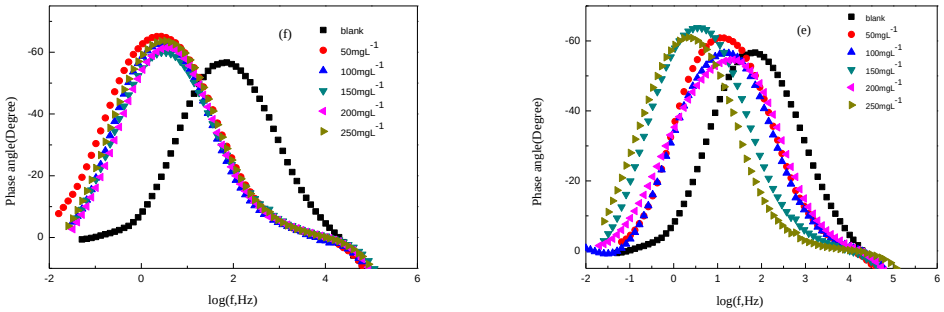

Figure 4. Nyquist (a, b) and Bode (c, d ,e, f) plots for the N80 carbon steel exposed in 3wt% NaCl solution in the absence and presence of different dosages of histidine and histidine dimer at 298 K (a, c, e-histidine, b, d, f -histidine dimer)

Nyquist (a, b) and Bode (c, d, e, f) plots for N80 carbon steel after immersion in 3 wt% NaCl solution with different dosages of histidine and histidine dimer are shown in Fig 4. As shown in Fig 4(a, b), all the plots have a single depressed semicircle appearance in the complex impedance plane with the centre up the real axis, and the diameter of the semicircle increases with an increasing concentration of inhibitors, indicating that the corrosion resistance of carbon steel was increased. From Fig 4(c, d, e, f), it should be noted that although the shapes of these graphs are similar throughout the experiment, adding the inhibitor does not change the corrosion mechanism[43].

Table 3. The parameters of electrochemical impedance spectroscopy for N80 carbon steel in the 3 wt% NaCl solution with various concentrations of histidine and histidine dimer at 298 K.

Inhibitors	C/mg·L^{-1}	R_s/Ω·cm^2	Q_{dl}/(F/ cm^2)	n/(0<n<1)	R_{ct}/Ω·cm^2	η_z/%
Histidine	0	5.4	2.2×10^{-4}	8.1×10^{-1}	197.8	--
	50	10.1	3.1×10^{-4}	8.3×10^{-1}	566.7	65.1
	100	14.1	2.6×10^{-4}	8.0×10^{-1}	743.1	734
	150	14.3	7.5×10^{-4}	8.4×10^{-1}	837.5	76.4
	200	11.5	6.7×10^{-4}	8.4×10^{-1}	894.6	77.9
	250	12.4	7.1×10^{-4}	8.3×10^{-1}	1020.0	80.6
Histidine dimer	50	14.1	6.9×10^{-4}	8.3×10^{-1}	727.3	72.8
	100	13.9	7.9×10^{-4}	8.0×10^{-1}	793.2	75.1
	150	12.3	3.0×10^{-4}	7.6×10^{-1}	987.4	80.0
	200	10.1	9.0×10^{-4}	8.2×10^{-1}	1163.0	83.0
	250	25.1	6.3×10^{-4}	8.3×10^{-1}	1285.0	84.7

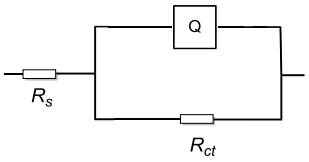

Figure 5. Electrical equivalent circuit model of EIS(Rs--solution resistance; Rct--charge-transfer resistance; and Q-- constant phase element of electrical double layer.)

The electrical equivalent circuits (EECs) based on impedance spectra are shown in Fig 5. The EIS data included the solution resistance (Rs) and charge transfer resistance (Rct) in a parallel combination with a constant phase element (Q). We used the constant phase to replace the double layer capacitance (Q_{dl}) to obtain a more accurate and representative fit. Table 3 shows the corresponding fitting data. The values of Rct were increased due to the addition of a different concentration of histidine compared to the blank solution, and the inhibitors' effectiveness also increased. This indicated that the addition of corrosion inhibitor molecules could be absorbed on the surface of the steel sheet and gradually form an organic adsorption layer to replace the water molecule layer and mitigate the dissolution of metals to inhibit corrosion [8, 44]. The organic layer between the metal surface and solution was generally considered an electrical double capacitor. Q_{dl} decreased with the increase of inhibitor concentration, which represented the increase in the thickness of the electric double capacitance layer and the decrease of the dielectric constant. R_s shows that the addition of corrosion inhibitor was much higher than the blank sample and was increased with increasing concentrations of inhibitor, indicating that the density of the corrosion inhibitor film increased[45]. The maximum inhibition efficiency (η_z/%) reached 80.60% and 84.61% at 0.25g/L of histidine and histidine dimer, respectively. The corrosion inhibition efficiency was similar to that obtained by the weight loss experiment. Based on EIS, the histidine dimer showed a better inhibitory performance than histidine for N80 steel in a 3 wt% NaCl solution.

3.4 Metal morphological analysis

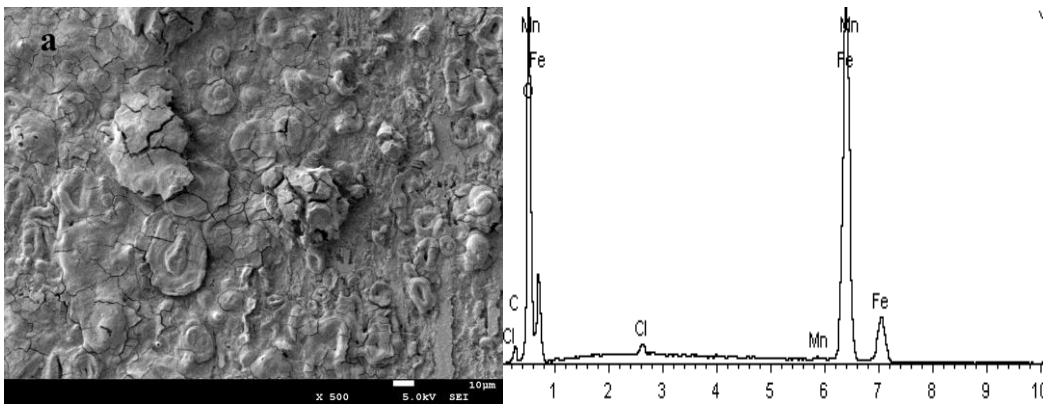

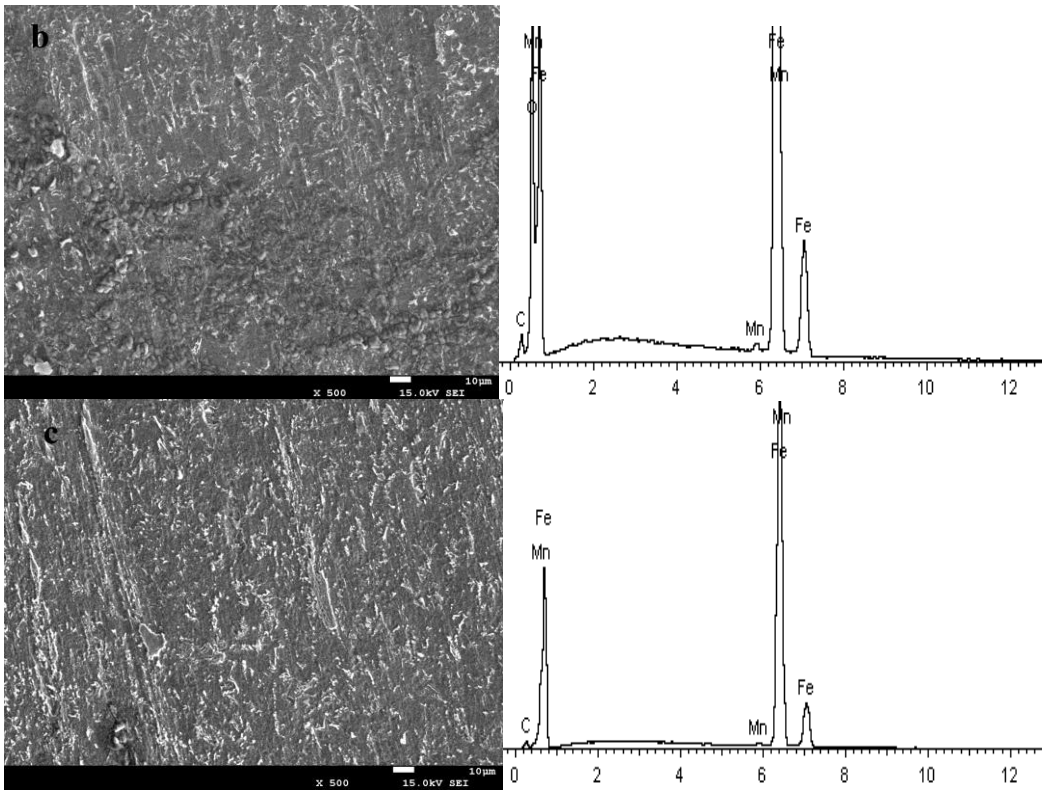

Figure 6. SEM images and EDS spectra of (a) blank, (b) 200mg/L histidine and (c) 200mg/L histidine dimer.

To observe the surface characterization of corroded N80 steel in 3 wt% NaCl solution, scanning electron microscopy (SEM) and energy dispersive spectroscopy (EDS) were applied on the uninhibited and inhibited N80 steel in this experiment. As shown in Fig 6(a), the metal surface was seriously damaged by localized corrosion in non-inhibitive solution. In the presence of histidine and the histidine dimer (Fig 6(b, c)), the surface of the N80 steel sheet uniformly showed little corrosion. Moreover, the percentages of atoms studied by EDS are listed in Table 4. The results indicated that along with addition of histidine and the histidine dimer, oxygen atom of the N80 steel surface decrease and even disappear compared to the unprotected steel, indicating a protective layer was formed on the carbon steel surface and was preventing the steel surface getting further corroded. The change of the oxygen atom reflects the histidine dimer was a better inhibitor compare to histidine[46, 47]. SEM and EDS experiments illustrated that histidine and the histidine dimer both impede the corrosion process of N80 steel in sodium chloride solution and exhibit good inhibition.

Table 4. The percentages of atoms studied by EDS

Atomic(%)	C	O	Fe	Mn	Cl
Blank	13.6	59	26.6	0.3	0.4
Histidine	1.5	44.7	53.4	0.4	--
Histidine Dimer	2.8	--	96.5	0.6	--

3.5 X-ray photoelectron spectroscopy (XPS)

Fig 7 shows the XPS spectrum of N80 steel after it was immersed 72 hours in 3 wt% NaCl solution with 0.20 g/L histidine and 0.2 g/L histidine dimer. As shown in Fig 7 (a), Fe, C, and O peaks appeared in the XPS spectrum of histidine.

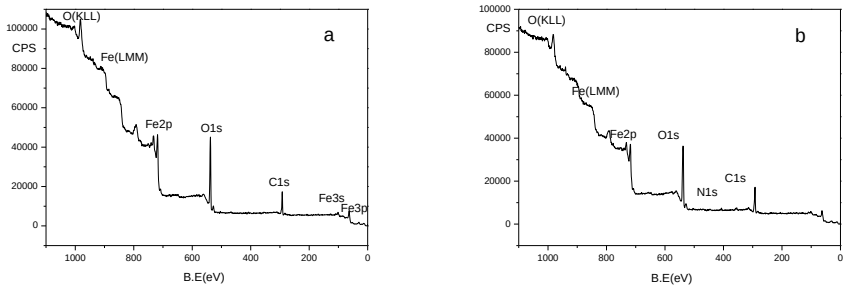

Figure 7. XPS spectra for Histidine and Histidine dimer on N80 steel (a: Histidine, b:Histidine dimer)

Besides the Fe, C, and O peaks, there were N peaks in the XPS spectrum of the histidine dimer (shown in Fig 7 (b)). This demonstrates that histidine dimer adsorbs on the N80 steel surface[48, 49]. Moreover, Fig.8 displays the C1s and N1s spectra for N80 carbon steel treated with histidine dimer. In the C1s spectra, the peak at 284.6 eV corresponded to C-C and C-H chemical bonds in aromatic hydrocarbons. The peaks at 286.0 eV and 288.0 eV corresponded to C=O and N-C=O bonds[50]. In the N1s spectra, the appearance of the peaks in the region of 398.8, 399.7 and 401.4 eV corresponded to the chemical bonds of N-Fe, N-C and NH-C=O, respectively. The appearance of these chemical bonds could also represent the adsorption of the histidine dimer on the surface of N80 steel[51].

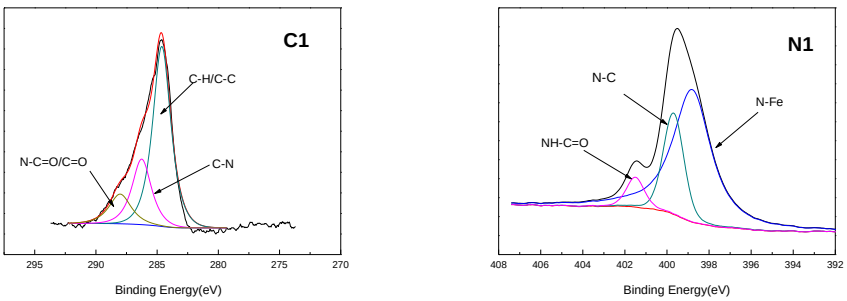

Figure 8. C1s and N1s spectra for Histidine Dimer treated on N80 carbon steel

3.6 Adsorption property

The adsorption isotherm (Langmuir, Temkin and Frumkin.) to describe the adsorption process of histidine and histidine dimer, substituting the experimental data into the eq.7, it found that the adsorption of histidine and histidine dimer on N80 steel obey the Langmuir adsorption isotherm.

$$C_i/\theta = 1/K_{ads} + C_i \quad (7)$$

Where, θ is the surface coverage listed in Table 1. K_{ads} and C_i are the equilibrium constant for adsorption- desorption process and the inhibitor concentration, respectively.

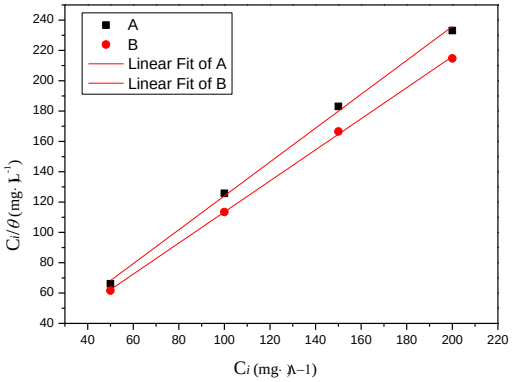

Figure 9. Langmuir adsorption plots for N80 steel in 3wt% NaCl solution at 298K in presence of different concentrations of (A) histidine and (B) histidine dimer.

The linear relationships of C/θ vs. C are depicted in Fig. 9. The linear correlation coefficients of the fitted data were 0.9976 and 0.9994, respectively. This confirms that the adsorption of histidine and the histidine dimer on the N80 surface obeys the Langmuir adsorption isotherm model[52]. The value of K_{ads} for histidine and the histidine dimer approach 1.2501×10^4 and 2.6497×10^4, respectively. The adsorption-desorption equilibrium constant K_{ads} was employed to evaluate the standard Gibbs free energy (ΔG^0_{ads}) of adsorption through Eq. (8).

$$\Delta G^0_{ads} = -RT\ln(55.5K_{ads}) \quad (8)$$

Where R represents the universal gas constant (8.314J·mol^{-1}·K^{-1}), T is the temperature (298K) and 55.5 mol·L^{-1} is the molar concentration of water in the solution.

Generally, the value of $\Delta G°_{ads}$ was below 20 kJ·mol^{-1}, which corresponded to physisorption, and when beyond 40 kJ·mol^{-1}, the adsorption was dominated by chemisorption resulting from the coordination of the corrosion inhibitor with the metal [53]. The values of $\Delta G°_{ads}$ for histidine and the histidine dimer were -33.32 kJ·mol^{-1} and -35.18 kJ·mol^{-1}, respectively. This illustrated that the histidine and histidine dimer adsorbed on N80 steel through both physisorption and chemisorption.

3.7 Quantum chemical calculation methods

The optimized structures of histidine and the histidine dimer and the optimized frontier molecular orbitals of histidine and the histidine dimer are displayed in Fig 10 and Fig 11. This reveals that the HOMO of histidine was mainly in the vicinity of the C-H bond and C=O bond and the LOMO was near the imidazole ring. The HOMO of histidine dimer occupied an imidazole ring and the LOMO

was mainly located at the amide bond. This illustrated that histidine and the histidine dimer are preferentially adsorbed on the metal surface by amide bonds and imidazole rings and form a more stable and more compact protective layer to block corrosion and further decrease the occurrence of corrosion.

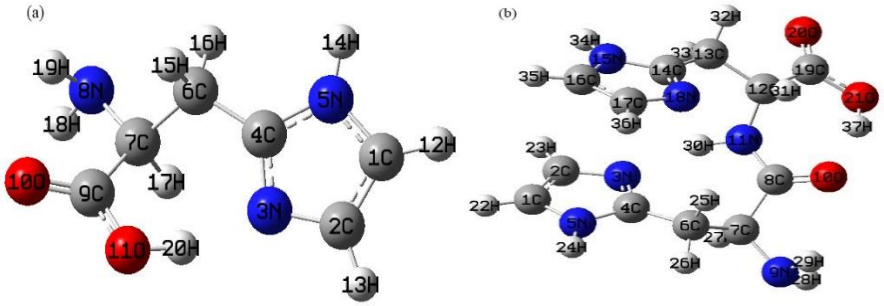

Figure 10. Optimized structures of (a)histidine and (b) histidine dimer

(a)

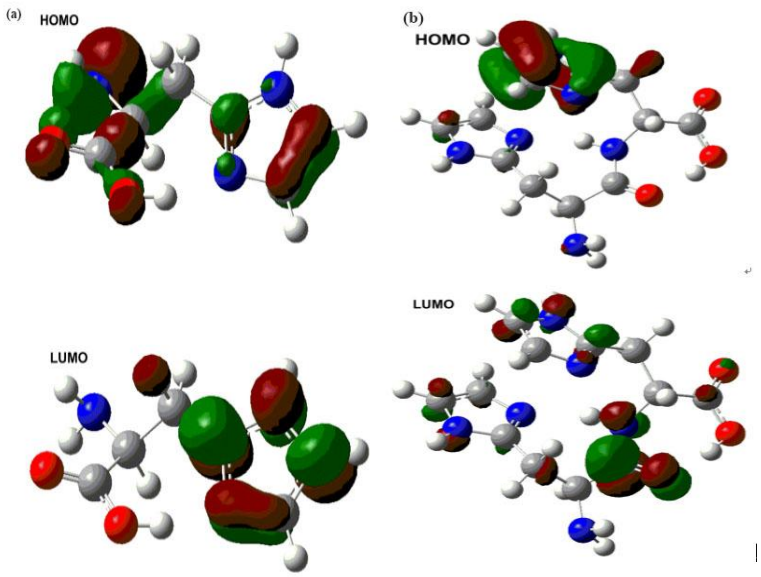

Figure 11. The frontier molecular orbitals (HOMO and LUMO) for optimized Histidine(a) and Histidine dimer(b) molecules.

Table 5. Quantum chemical parameters calculated using the Gaussian 09 program package with B3LYP/6–31 G (d, p) basis set for Histidine and Histidine dimer

Inhibitor	Total energy (a. u.)	E_{HOMO} (eV)	E_{LUMO}(eV)	η (eV)	ΔE(ev)	μ (Debye)	ΔN
Histidine	-548.6	-6.7	-9.4×10^{-2}	5.2	6.6	3.4	5.4×10^{-1}
Dimer	-1021.5	-6.4	-5.8×10^{-2}	4.8	6.3	3.3	6.0×10^{-1}

The calculated E_{HOMO}, E_{LUMO}, η, ΔE μ and ΔN values are given in Table 5. The ΔN values represent the direction of electron transfer (when $\Delta N<0$, electron transfer occurs from the Fe surface to the molecule, not from the molecule to the Fe surface)[54]. According to previous studies[55], when ΔN is less than 3.6, the inhibition efficiency increases with increased electron-donating capability of the metallic surface inhibitor. As shown in Table 5, the ΔN of investigated inhibitors is less than 3.6 and positive, indicating that the inhibitor molecules can provide electrons to form a coordinate bond on the metal surface. However, the ΔN value of the histidine dimer is slightly greater than that of histidine, which implied that the histidine dimer has a greater ability to donate electrons to the metal surface [56]. The dipole moment (μ) is another index that is mainly used to predict the direction of the inhibition of the corrosion process .Chemical hardness (η) is associated with selectivity, which can measure the capacity of an atom to prevent charge transfer. E_{HOMO} is related to the power of the molecule to provide electrons. A high E_{HOMO} reveals that the molecule tends to donate electrons and accept a molecule's LUMO orbital.

Table 5 shows that all E_{HOMO} values were negative. Moreover, Arslan [57] indicated that the negative E_{HOMO} values were evidence of physical adsorption, and low E_{LUMO} values suggested that the electron receptiveness of the molecule was very high. The histidine dimer had a lower E_{LUMO} than histidine (Table 5). The energy gap (ΔE) and the value difference of E_{HOMO} and E_{LUMO} ($\Delta E= E_{LUMO}-E_{HOMO}$) are important parameters to determine the reactivity of a molecule. In comparison, the ΔE in Table 5 showed that the values of the histidine dimer were lower than those of histidine, which revealed that the histidine dimer is adsorbed on the steel surface more strongly than histidine. Therefore, the above results are in agreement with the empirical findings.

4. CONCLUSION

Histidine dimmers were successfully synthesized and could adsorb on the N80 steel surface and hinder anodic and cathodic reactions in 3% NaCl solution. At the same time, the inhibition efficiency of the dimer was better than that of histidine according to weight loss measurements. At the concentration of 250 mg/L histidine dimer, the inhibition efficiency of the histidine dimer could reach a maximum of 94.09%. According to electrochemical experiments, histidine and the histidine dimer were considered mixed-type corrosion inhibitors with a predominantly cathodic action. The analysis of the consequences of the surface morphology and elemental composition of corroded N80 steel by Scanning Electron Microscopy (SEM), energy disperse spectrometry (EDS) and X-Ray Photoelectron Spectroscopy (XPS) further certified that histidine and the histidine dimer adsorbed and formed a protective layer on the carbon steel surface in the 3% NaCl solution, which isolated the active sites and impeded the occurrence of corrosion. The adsorption of histidine and the histidine dimer was confirmed to follow the Langmuir isotherm model. Comparing the inhibition effectiveness of the histidine dimer and histidine by quantum chemical calculation methods revealed that their inhibition behaviour was closely related to orbital energies (E_{HOMO} and E_{LUMO}), energy gap (ΔE), dipole moment, and the fraction of electrons transferred. The results showed that the histidine dimer exhibits a better inhibition performance than histidine.

ACKNOWLEDGEMENT
This study was funded by National Natural Science Foundation of China (51774245), Sichuan Province sci-tech Supported project (2015RZ0023), Youth science and technology creative group fund of Southwest Petroleum University (2015CXTD03),and The majorly cultivated project of sci-tech achievements transition (15CZ0005) from the education department in Sichuan Province.

CONFLICT OF INTEREST
The authors declare that they have no conflict of interest.

References

1. R. Fuchs-Godec, M.G. Pavlovic, *Corros. Sci.*, 58 (2012) 192.
2. Y.F. Cheng, M. Wilmott, J.L. Luo, *Appl. Surf. Sc*i., 152 (1999) 161.
3. Y.F. Cheng, J.L. Luo, *Br. Corros. J.*, 35 (2000) 125.
4. M.G. Alvarez, J.R. Galvele, *Corros. Sci*., 24 (1984) 27.
5. L. Cáceres, T. Vargas, L. Herrera, *Corros. Sci*., 49 (2007) 3168.
6. M. Ghahari, D. Krouse, N. Laycock, T. Rayment, C. Padovani, M. Stampanoni, F. Marone, R. Mokso, A.J. Davenport, *Corros. Sci*., 100 (2015) 23.
7. L. Cáceres, T. Vargas, L. Herrera, *Corros. Sci.*, 51 (2009) 971.
8. S. John, M. Kuruvilla, A. Joseph, *RSC Adv*., 3 (2013) 8929.
9. Y. Sasikumar, A.S. Adekunle, L.O. Olasunkanmi, I. Bahadur, R. Baskar, M.M. Kabanda, I.B. Obot, E.E. Ebenso, *J. Mol. Liq*., 211 (2015) 105.
10. G. Trabanelli, *Corrosion*, 47 (1991) 410.
11. I. Ahamad, M.A. Quraishi, *Corros. Sci.*, 51 (2009) 2006.
12. O. Benali, L. Larabi, M. Traisnel, L. Gengembre, Y. Harek, Appl. Surf. Sci., 253 (2007) 6130.
13. F. Bentiss, M. Lebrini, M. Lagrenée, *Corros. Sci*., 47 (2005) 2915.
14. J. Cruz, R. MartíNez, J. Genesca, E. GarcíA-Ochoa, *J. Electroanal. Chem.*, 566 (2004) 111.
15. B. Hamah-Ali, B.S. Ali, R. Yusoff, M.K. Aroua, *Int. J. Electrochem. Sci.*, 6 (2011) 181.
16. M.A. Quraishi, N.A. Sardar, H.A. Ali, *Corrosion*, 58 (4)(2002) 317.
17. N.A.F. Al-Rawashdeh, *Int. J. Electrochem. Sci.*, (2017) 8535.
18. M.I. Awad, A.F. Saad, M.R. Shaaban, B.A. Al Jahdaly, O.A. Hazazi, *Int. J. Electrochem. Sci.*, 12 (2017) 1657.
19. H. Ashassi-Sorkhabi, M.R. Majidi, K. Seyyedi, *Appl. Surf. Sci.*, 225 (2004) 176.
20. Q. Deng, X.P. He, H.W. Shi, B.Q. Chen, G. Liu, Y. Tang, Y.T. Long, G.R. Chen, K. Chen, *Ind. Eng. Chem. Res.*, 51(21) (2012) 7160.
21. K.F. Khaled, S.R. Al-Mhyawi, *Int. J. Electrochem. Sci*., 8 (2013) 4055.
22. O. Olivares-Xometl, N.V. Likhanova, M.A. Domínguez-Aguilar, E. Arce, H. Dorantes, P. Arellanes-Lozada, *Mater. Chem. Phys.*, 110 (2008) 344.
23. R.N. Ranjanabanerjee, M M,Indian *J. Chem. Technol.*, 17 (2010) 176.
24. M.A. Amin, K.F. Khaled, Q. Mohsen, H.A. Arida, *Corros. Sci.*, 52 (2010) 1684.
25. G.L.F. Mendonça, S.N. Costa, V.N. Freire, P.N.S. Casciano, A.N. Correia, P.D. Lima-Neto, *Corros. Sci.*, 115(2017)41.
26. D.Q. Zhang, Q.R. Cai, X.M. He, L.X. Gao, G.D. Zhou, *Mater. Chem. Phys*., 112 (2008) 353.
27. M.M. El-Rabiee, N.H. Helal, G.M.A. El-Hafez, W.A. Badawy, *J. Alloys Compd.*, 459 (2008) 466.
28. W.A. Badawy, K.M. Ismail, A.M. Fathi, *Electrochim. Acta*, 51 (2006) 4182.
29. J. Aljourani, K. Raeissi, M.A. Golozar, *Corros. Sci*., 51 (2009) 1836.
30. I.B. Obot, N.O. Obi-Egbedi, S.A. Umoren, *Corros. Sci.*, 51 (2009) 276.
31. M.L. Zheludkevich, K.A. Yasakau, S.K. Poznyak, M.G.S. Ferreira, *Corros. Sci.*, 47 (2005) 3368.
32. J. Fu, S. Li, Y. Wang, L. Cao, L. Lu, *J. Mater. Sci.*, 45 (2010) 6255.
33. M. Bobina, A. Kellenberger, J.P. Millet, C. Muntean, N. Vaszilcsin, *Corros. Sci.*, 69 (2013) 389.

34. A.S. Fouda, M.A. Ismael, R.M.A. Shahba, L.A. Kamel, A.A. El-Nagggar, *Int. J. Electrochem. Sci*., 12 (2017) 3361.
35. A.M. Fekry, R.R. Mohamed, *Electrochim. Acta*, 55 (2010) 1933.
36. K.F. Khaled, *Corros. Sci*., 52 (2010) 3225.
37. N.A. Negma, N.G.K. B, E.A.B. A, M.A. Mohammedc, *Corros. Sci.*, 65 (2012) 94.
38. A. Kosari, M.H. Moayed, A. Davoodi, R. Parvizi, M. Momeni, H. Eshghi, H. Moradi, *Corros. Sci.*, 78 (2014) 138.
39. F. Zhang, Y. Tang, Z. Cao, W. Jing, Z. Wu, Y. Chen, *Corros. Sci.*, 61 (2012) 1.
40. A.S. Fouda, L.H. Madkour, A.A. El-Shafei, S.A.A. El-Maksoud, *Bull. Korean Chem. Soc.,* 16 (1995) 454.
41. I. Ahamad, R. Prasad, M.A. Quraishi, *Corros. Sci.*, 52 (2010) 1472.
42. P.M. Krishnegowda, V.T. Venkatesha, P.K.M. Krishnegowda, S.B. Shivayogiraju, *Ind. Eng. Chem. Res.*, 52 (2013) 722.
43. Y. Fan, Y. He, P. Luo, T. Shi, X. Chen, *J. Electrochem. Soc.*, 163 (2016) D68.
44. E.E. Ebenso, M.M. Kabanda, T. Arslan, M. Saracoglu, F. Kandemirli, L.C. Murulana, A.K. Singh, S.K. Shukla, B. Hammouti, K.F. Khaled, *Int. J. Electrochem. Sci*., 7 (2012) 5643.
45. M.A. Ameer, A.M. Fekry, *Int. J. Hydrogen Energy*, 35 (2010) 11387.
46. P. Mourya, S. Banerjee, R.B. Rastogi, M.M. Singh, *Ind. Eng. Chem. Res.*, 52 (2013) 12733.
47. R. Kumar, O.S. Yadav, G. Singh, *J. Mol. Liq.*, 237 (2017)413.
48. F. Bentiss, M. Traisnel, H. Vezin, H.F. Hildebrand, M. Lagrenée, *Corros. Sci.*, 46 (2004) 2781.
49. F. Cheng, *Corrosion*, 72(4)(2016)472.
50. O. Olivares, N.V. Likhanova, B. Gómez, J. Navarrete, M.E. Llanos-Serrano, E. Arce, J.M. Hallen, *Appl. Surf. Sci*., 252 (2006) 2894.
51. S.R. Kelemen, A. M. Afeworki, M.L. Gorbaty, A.D. Cohen, *Energy Fuels*, 16 (2002) 1450.
52. N.A. Negm, N.G. Kandile, I.A. Aiad, M.A. Mohammad, *Colloids Surf.*, A, 391 (2011) 224.
53. Y.Y. Jiang, Y. Chen, Z.Y. Ye, H. Chen, Z. Zhang, J.Q. Zhang, C.N. Cao, *Corrosion*, 69 (2013) 672.
54. A. Kokalj, Electrochim. Acta, 56 (2011) 745.
55. N.O. Eddy, F.E. Awe, C.E. Gimba, N.O. Ibisi, E.E. Ebenso, QSAR, *Int. J. Electrochem. Sci*., 6 (2011) 931.
56. G. Gece, *Corros. Sci.*, 50 (2008) 2981.
57. E.E. Ebenso, T. Arslan, F. Kandemi, *Int. J. Quantum Chem*., 110 (2010) 2614.